This paper describes objective technical results and analysis. Any subjective views or opinions that might be expressed in the paper do not necessarily represent the views of the U.S. Department of Energy or the United States Government.

SAND2021-15134C

Mid-Infrared Laser-Absorption-Spectroscopy Measurements of Temperature, Pressure, and NO $X^2\Pi_{1/2}$ at 500 kHz in Shock-Heated Air

Morgan D. Ruesch*, Jonathan J. Gilvey†, Christopher S. Goldenstein‡
Purdue University, West Lafayette, IN, United States

Kyle A. Daniel§, Charley R. Downing¶, Kyle P. Lynch ‖, Justin L. Wagner**
Sandia National Laboratories, Albuquerque, NM, United States

This work presents a high-speed laser-absorption-spectroscopy diagnostic capable of measuring temperature, pressure, and nitric oxide (NO) mole fraction in shock-heated air at a measurement rate of 500 kHz. This diagnostic was demonstrated in the High-Temperature Shock Tube (HST) facility at Sandia National Laboratories. The diagnostic utilizes a quantum-cascade laser to measure the absorbance spectra of two rovibrational transitions near 5.06 μm in the fundamental vibration bands (v'' = 0 and 1) of NO in its ground electronic state ($X^2\Pi_{1/2}$). Gas properties were determined using scanned-wavelength direct absorption and a recently established fitting method that utilizes a modified form of the time-domain molecular free-induction-decay signal (m-FID). This diagnostic was applied to acquire measurements in shock-heated air in the HST at temperatures ranging from approximately 2500 to 5500 K and pressures of 3 to 12 atm behind both incident and reflected shocks. The measurements agree well with the temperature predicted by NASA CEA and the pressure measured simultaneously using PCB pressure sensors. The measurements presented demonstrate that this diagnostic is capable of resolving the formation of NO in shock-heated air and the associated temperature change at the conditions studied.

I. Nomenclature

$A(t)$	=	m-FID signal
E_j"	=	lower-state energy of absorption transition j
$\mathcal{F}^{-1}$	=	inverse Fourier transform
I_0	=	incident light intensity
I_t	=	transmitted light intensity
J"	=	lower-state rotational quantum number
L	=	path length
P	=	pressure
S_j	=	linestrength of absorption transition j
T	=	temperature
v"	=	lower-state vibrational quantum number
X_i	=	mole fraction of absorbing species i
α	=	absorbance
γ_{NO-i}	=	collisional half-width of NO transition with collision partner i
ν	=	optical frequency
$\Delta\nu_c$	=	collisional full-width at half-maximum

*(Currently) Research Scientist, Combustion Research and Flow Technology, Inc., 6210 Keller's Church Rd., Pipersville, PA 18947
†Graduate Student, School of Mechanical Engineering, 585 Purdue Mall, West Lafayette, IN 47907
‡Assistant Professor, School of Mechanical Engineering, 585 Purdue Mall, West Lafayette, IN 47907, Senior Member AIAA
§Postdoctoral Appointee, Engineering Sciences Center
¶Principal Technologist, Engineering Sciences Center
‖Senior Member of the Technical Staff, Engineering Sciences Center, Senior Member AIAA
**Principal Member of the Technical Staff, Engineering Sciences Center, Associate Fellow AIAA

Sandia National Laboratories is a multimission laboratory managed and operated by National Technology & Engineering Solutions of Sandia, LLC, a wholly owned subsidiary of Honeywell International Inc., for the U.S. Department of Energy's National Nuclear Security Administration under contract DE-NA0003525.

ϕ_j = lineshape function for transition j

II. Introduction

The high enthalpy of hypersonic air flows has a dramatic impact on the aerodynamics and thermal management of an aircraft [1]. However, the complex thermochemical processes occurring in air at hypersonic flight conditions are still not well understood. As a result, there remains a significant need for experimental characterization of the thermochemical processes which are relevant to hypersonic flows to both inform and validate predictive tools.

For example, experiments are needed to characterize the dissociation rates of many species, which are still not well understood. Johnston and Brandis [2] developed a chemical kinetic model for CO_2-N_2 mixtures by tuning the dissociation rate of various species to minimize the difference between simulated and experimental radiance measurements at the NASA EAST shock tube facility. The simulated radiance was found to be most sensitive to the dissociation rates of CO_2, CO, O_2, and NO. The model that they developed using the tuned dissociation rates predicted significantly lower non-equilibrium radiance than previous models and gave improved agreement with experiments.

The High-temperature Shock-Tube (HST) at Sandia National Laboratories is a free-piston shock tube which is capable of generating extreme aerodynamic conditions behind shock waves [3]. Further, this facility provides the capability to create high-enthalpy stagnation gases as a reservoir for the recently constructed Hypersonic Reflected Shock Tunnel (HST-R) [4]. These facilities have motivated the development of diagnostics capable of making measurements of thermochemical conditions in high-temperature air.

Characterization of the thermochemical state of both the reservoir and freestream flow of a hypersonic shock tunnel is required to accurately compare experiments to simulations. For example, Nompelis *et al.* investigated discrepancies in experimental and modeled heat-transfer rates, for a double-cone exposed to hypersonic flow, at the CUBRC LENS facility [5]. The authors found that the vibrational modes of nitrogen froze near the nozzle throat, resulting in elevated vibrational temperatures in the freestream. When the vibrational freezing of N_2 in the nozzle was accounted for the heat-transfer rate to the model was reduced by 20% and came into agreement with experiments. Thus, to accurately compare experimental data to simulations, the thermochemical state of the reservoir gas and the freestream exiting the nozzle, at hypersonic facilities, must be characterized.

Experimental measurements of gas conditions in hypersonic flows are challenging as many techniques are intrusive or do not provide quantitative thermodynamic information. Spectroscopy based measurements, on the other hand, can measure gas conditions such as temperature, pressure, state-specific species mole fraction, and velocity in harsh environments [6–8]. However, this is a challenge in air as molecular nitrogen and oxygen exhibit spectroscopic transitions deep in the ultraviolet that are difficult to access with conventional laser systems. Alternatively, nitric oxide (NO) has strong rovibrational transitions in the infrared which can now be easily accessed by tunable semiconductor lasers (e.g., interband cascade lasers (ICLs) and quantum-cascade lasers (QCLs)). NO is formed in significant quantities in air at high temperatures due to the well known Zeldovich mechanism [9] making it an attractive candidate for characterizing the gas conditions of high-temperature air via laser absorption spectroscopy [10–13]. Other spectroscopic techniques utilizing NO have been applied to study high-enthalpy gases including emission and laser-induced fluorescence [14–17] which operate in the UV.

LAS is a particularly attractive technique due to the ability to provide quantitative, non-intrusive measurements of temperature and species or state concentrations. Some of the first implementations of NO-based LAS were demonstrated using either a carbon monoxide laser [18, 19] or cryogenically cooled diode lasers [20–23]. Advances in laser technology have provided the capability to make measurements using more practical (i.e., thermoelectrically cooled) semiconductor lasers (e.g., tunable diode lasers). Diode lasers have been used to measure the absorption spectra of NO using the first [24] and second [25] overtone bands of NO in the near-infrared. More recently, QCLs have been utilized for measurements of NO using much stronger transitions in the fundamental vibration bands located in the mid-infrared near 5.2 μm [10, 11, 26–31]. Spearrin *et al.* [10] and Almodovar *et al.* [30] both demonstrated diagnostics capable of measuring NO in high-enthalpy gases using various types of QCLs. Parker *et al.* demonstrated the use of a QCL in the free stream of several hypersonic wind tunnels at the CUBRC facility for measurements of NO and velocity [27, 28]. Recently, several studies have been performed to characterize the free stream of the T5 reflected shock tunnel at Caltech including measurements of rotational and vibrational temperatures of NO, velocity, and NO partial pressure, as well as other gas species [11–13].

Although NO has a rich history of measurements in hypersonic facilities and high-enthalpy air, all previous studies have made measurements at temperatures below 3000 K. Since gas temperatures in hypersonic flows can well exceed 3000 K, it is important to develop diagnostics capable of making measurements at higher temperatures than those

previously studied. In addition, most diagnostics have been incapable of providing fast enough measurement rates to resolve chemical and/or thermal non-equilibrium at these high temperatures. The objective of this study was to develop and apply an LAS diagnostic capable of making near-MHz measurements of temperature, pressure, and NO mole fraction in the HST at Sandia National Laboratories at temperatures up to ≈5500 K. This work was part of an ongoing effort to characterize the HST facility and develop novel diagnostics relevant to hypersonic flows.

III. Fundamentals of Absorption Spectroscopy

In LAS, laser light is directed through an absorbing gas and the transmitted light intensity is measured as a function of optical frequency. The absorbance can then be determined according to the Beer-Lambert Law given in Eq. 1.

$$\frac{I_t}{I_0} = exp[-\alpha(\nu)] \tag{1}$$

If the gas conditions are uniform along the line-of-sight, the gas properties of a test gas are then related to the absorbance at a specific optical frequency according to Eq. 2.

$$\alpha(\nu) = \sum_j S_j(T) P X_i L \phi_j(\nu) \tag{2}$$

The Voigt profile is often used to model the lineshape of a transition to account for both Doppler and collisional broadening, assuming they are not coupled.

Various methods can be employed to determine the gas properties from a measured absorbance spectra. Thermometry can be performed by measuring the absorbance spectra of two or more transitions with unique E". As a result, the temperature sensitivity of the diagnostic is directly related to the E" of the transitions [32] and it is desirable to use transitions with a large difference in E". If the collisional broadening can be accurately modelled, the measured collisional width can be used to measure pressure using Eq. 3.

$$\Delta\nu_c = P \sum_{i=1}^{n} X_i 2\gamma_{NO-i} \tag{3}$$

With temperature, pressure, and path length known, the mole fraction of the absorbing species can then be determined from the magnitude of the measured absorbance spectra, or integrated area.

A. Modified Free-Induction-Decay Signal

Correct determination of the incident light intensity is one of the primary challenges to making accurate measurements using direct absorption spectroscopy. Recently, cepstral analysis has been demonstrated for use with LAS to determine a modified form of the time-domain molecular free-induction-decay (m-FID) signal [33, 34]. This method was first adapted for use with scanned-wavelength direct absorption using tunable, narrow bandwidth lasers (e.g. DFB QCLs) by Goldenstein *et al.* [34] and further refined by Li *et al.* [35]. In this method, the m-FID signal is determined by converting the measured transmitted intensity as a function of optical frequency into the time domain using an inverse Fourier transform. Gas properties are then determined by least-squares fitting a simulated m-FID signal that is comprised of the assumed incident intensity (or "baseline") and simulated absorbance spectrum. This method was shown to be insensitive to error in the baseline as the contribution to the m-FID signal from baseline error decays rapidly in the time domain and can be ignored by the fitting routine.

The m-FID signal ($A(t)$) of a measured transmitted intensity can be calculated by applying an inverse Fourier transform to the Beer-Lambert law (Eq. 1) as shown in Eq. 4 and Eq. 5.

$$A(\nu) = -ln(I_t(\nu)) = \alpha(\nu) - ln(I_0(\nu)) \tag{4}$$

$$A(t) = \mathcal{F}^{-1}[A(\nu)] = \mathcal{F}^{-1}[\alpha(\nu)] + \mathcal{F}^{-1}[-ln(I_0(\nu))] \tag{5}$$

The m-FID signal in Eq. 5 is comprised of the addition of two terms. The first term is only a function of the absorbance spectrum of the test gas, while the second term depends on the assumed incident intensity. Slowly varying errors in the second term (i.e., in the baseline) will rapidly decay to zero in the time domain. This occurs much more rapidly than the rate at which the m-FID signal from the first term (i.e., the absorbance) decays. As a result, error in the assumed

baseline can be filtered out by only fitting to points in the m-FID signal after errors in the signal from the baseline have decayed close to zero.

IV. Line Selection

The LAS diagnostic utilizes the R(0,36.5) and R(1,55.5) transitions of the $X^2\Pi_{1/2}$ subband of the ground electronic state of NO near 1976 cm^{-1} where the nomenclature R(v", J") refers to the lower vibrational (v") and rotational (J") quantum numbers in the R branch. Figure 1 (left) shows the absorbance spectra of the fundamental vibration bands of NO at a temperature of 4000 K and a pressure of 1 atm. The spectra were calculated using the HITEMP 2019 database [36, 37] and an in-house model for determining the partition function of NO via a sum over states at an arbitrary temperature. The latter was particularly important for conditions above 5000 K where published values for the partition function stop (e.g., ExoMol [38]). The vertical dashed line indicates the location of the transitions of interest in this study. Figure 1 (right) shows the absorbance spectra of the transitions of interest at a temperature of 4000 K, X_{NO} of 0.05, pressures of 1 (solid lines) and 5 (dashed lines) atm, and a path length of 7.3 cm. The absorbance spectra of CO and H_2O are also included assuming a mole fraction of 0.01. These transitions were selected for several reasons. (1) The linestrengths of these lines are strong enough to make single pass measurements in the HST in the desired temperature range (2500-5500 K). (2) These lines have minimal interference from CO and H_2O at the target gas conditions. Although, contamination from H_2O and CO was investigated and found to be undetectable in the HST using these wavelengths, particular care was taken to avoid interfering absorption lines of CO and H_2O since other free-piston shock-tube facilities have reported unanticipated contamination from CO and H_2O in their test gas [11, 12]. (3) The difference in E" between the two transitions is large (≈4750 cm^{-1}) providing excellent sensitivity to temperature. (4) The spacing between the transition line centers is near optimal for single-laser access at near-MHz scan rates. The line centers are close enough together requiring only one laser to scan over both transitions while still being separated enough that the transitions are easily distinguishable for measurements at elevated pressures (3-12 atm, see Figure 1 (right)). Finally, (5) the commercially available QCL, capable of emitting laser radiation at the wavelength of these transitions, had excellent wavelength tuning at high scan rates (100s of kHz) which, in addition to bias-tee circuitry, was critical to making measurements with sufficient time resolution in the HST. See section V.B for more discussion on the QCL used.

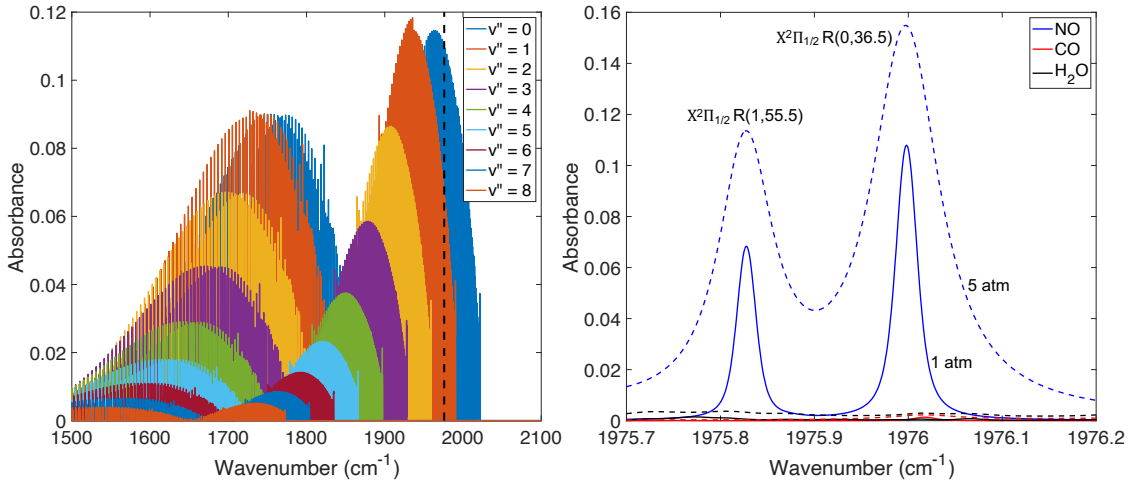

Fig. 1 (Left) Absorbance spectra of the fundamental vibration bands of NO with different v" at 4000 K, 1 atm, X_{NO} of 0.05, and a path length of 7.3 cm. The dashed line indicates the location of the lines targeted in this work. (Right) Absorbance spectra of the NO lines of interest at 1 and 5 atm, 4000 K, X_{NO} of 0.05, and a path length of 7.3 cm. Interference from CO and H_2O lines is also shown assuming a mole fraction of 0.01 for both species.

V. Experimental Methods

A. HST

The HST is a free-piston shock-tube facility, located at Sandia National Laboratories, which can generate strong shocks to produce simultaneous high-temperature and -pressure environments. The free-piston shock tube uses an 11.9-kg piston to isentropically compress the driver gas to a state with high-pressures (≈10 MPa) and -temperatures (≈2000 K). When combined with a light driver gas, such as helium, the HST is able to generate shocks that are much stronger compared to many traditional shock-tubes.

The driven section of the HST is equipped with multiple fast response PCB pressure sensors (113B24, 113B26) that monitor pressure and are used to measure the shock speed along the tube. A PCB model 483C signal conditioner was used to provide excitation voltage and signal amplification. The data was low-pass filtered using a Krohn-Hite model 2284 signal conditioner with a four-pole Butterworth filter and a cut-off frequency of 500 kHz. The data was sampled at 2 MHz using a computer DAQ system equipped with a NI PXIe-6376 module and recorded on a personal computer using an in-house LabView code.

Tests were performed in shock-heated air at temperatures from 2500 to 5500 K and pressures of approximately 3 to 12 atm. Measurements were made behind either the incident or reflected shock waves. When making measurements behind the reflected shock, the endwall was positioned to be only 6 mm from the measurement path. Thus, in all reflected-shock tests, the time between incident and reflected shock arrival was minimized. In tests where measurements were acquired behind the incident shock an endwall located approximately 180 mm further downstream was used to allow for longer test times. In all tests, dried air was used as the driven gas and the driver gas was helium, nitrogen, or a mixture of the two. Further details of the HST design and operation can be found in Lynch and Wagner [3].

B. LAS Diagnostic

A schematic of the experimental setup is shown in Figure 2. Measurements of temperature, pressure, and NO mole fraction were acquired using scanned-wavelength direct absorption (scanned-DA) with a distributed feedback QCL (ALPES Lasers) that has a maximum power of ≈50 mW. The laser was scanned over two transitions of NO at 500 kHz using injection-current tuning. In order to achieve a scan rate of 500 kHz, a bias-tee (SigaTek, SB12D2D) was implemented into the laser control setup similar to Nair *et al.* [39]. A laser controller (Arroyo 6310-QCL) was used for temperature control and to set the DC current of the laser. The modulation of the laser was controlled by a radio frequency (RF) signal from a function generator which was combined with the DC current from the laser controller in the bias-tee. Using a bias-tee in this manner enabled the RF modulation to bypass the laser controller which has limited bandwidth (200 kHz) allowing for higher modulation frequencies beyond the bandwidth of the controller to be used. The impact of implementing the bias-tee on the maximum peak-to-peak scan depth of the laser is shown in Figure 3. When modulating the laser current through the laser controller, the scan depth begins to rapidly drop as the

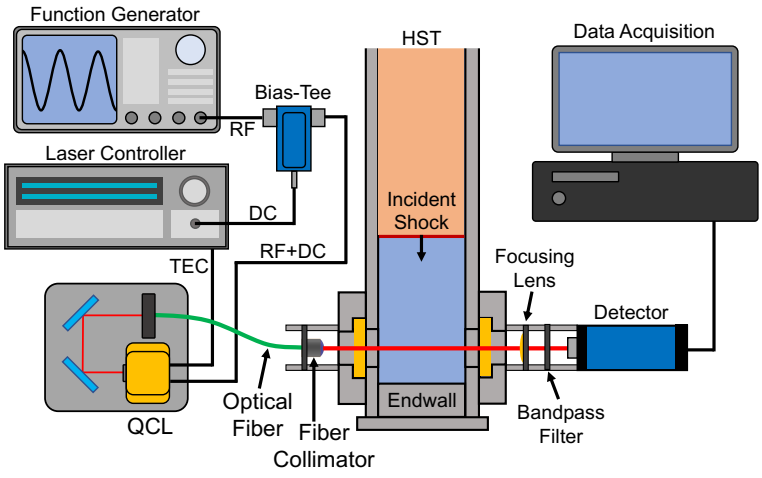

Fig. 2 Diagram of the experimental setup.

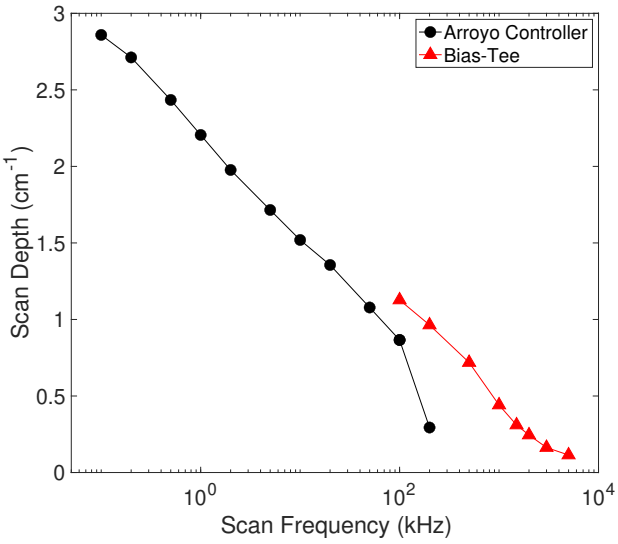

Fig. 3 The maximum peak-to-peak scan depth (i.e., amplitude) of the QCL as a function of scan frequency with and without the bias-tee.

scan frequency approaches the bandwidth of the controller. Implementing the bias-tee extended the scan frequencies at which the laser can be used to scan over both of the transitions of NO.

To make measurements in the HST, the laser was fiber coupled into a single-mode InF_3 fiber using an anti-reflective coated collimating lens to focus the beam into the fiber. Another collimating lens on the other end of the fiber was mounted to the window holder of the HST to direct the laser light through the test section of the shock tube. After passing through the test gas, the transmitted laser light was collected on a 250 MHz mercury-cadmium-telluride detector (Vigo Systems PVMI-2TE-8) mounted on the opposite window holder. The transmitted laser light was focused onto the detector with a 40 mm CaF_2 lens and passed through a 100 nm FWHM bandpass filter centered at 5.068 μm (Thorlabs, FB5068-100). The detector voltage was recorded at 3 GS/s using a 12-bit data acquisition system (GaGe CSE123G2). The wavelength scanning of the QCL was characterized using a 3-inch long germanium etalon with a free spectral range of $\approx$0.016 cm^{-1}.

VI. LAS Data Processing

During post processing, gas properties were determined using a nonlinear least-squares fitting routine to fit a simulated m-FID signal to the measured m-FID signal determined from the measured transmitted intensity of the laser. The simulated m-FID signal was comprised of a simulated absorbance spectra applied to an assumed incident intensity, obtained from a background measurement. The simulated absorbance spectra were calculated using the HITEMP 2019 database [36] and included all lines between 1971 and 1981 cm^{-1}. All the transitions within this range were included in the simulated absorbance to take into account any impact neighboring transitions had on the measured absorbance spectra.

An example of the measured transmitted and assumed incident light intensity for a single scan is shown in Figure 4 (left). The resulting m-FID signal from the measured transmitted intensity and the associated best-fit m-FID signal is shown in Figure 4 (middle). The measured and best-fit m-FID signals generally were in excellent agreement with residuals within $\approx$1%. For reference, the absorbance spectra associated with the measured and best-fit m-FID signals in Figure 4 (middle) are shown in Figure 4 (right). The use of the m-FID signal for the fitting routine is clearly able to capture the absorbance spectra well. In addition to rejecting errors in the baseline, utilizing this method was found to have several benefits compared to fitting to the absorbance spectra directly with a baseline correction [34]. These benefits included improved computational times for the fitting routine and improved precision in measured gas properties.

The free parameters of the least-squares fitting routine were temperature, pressure, partial pressure of NO, and the line center of the two transitions. The simulated m-FID signal was fit to points 3 through 46 of the measured m-FID signal to reject the signal from errors in the baseline, which decay rapidly within the first two data points. The pressure

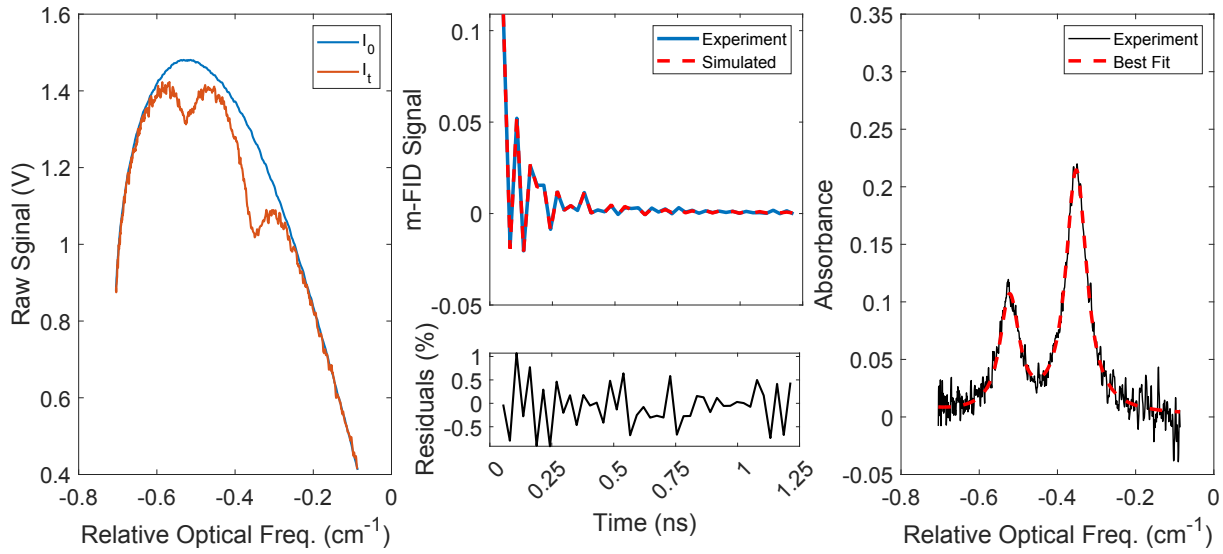

Fig. 4 (Left) An example single-scan measurement of transmitted light intensity with NO absorption present and the assumed incident intensity (i.e., baseline). (Middle) The m-FID signal from the measured transmitted intensity and the best-fit m-FID signal. (Right) The measured and best-fit absorbance spectra associated with the m-FID signals shown, for reference.

was determined by comparing the measured collisional width of the R(0,36.5) line to that predicted by HITEMP 2019. In addition, in the fitting routine, the collisional widths of the two transitions were constrained to be a ratio of each other that was dependent on the gas temperature. This ratio of the collisional widths as a function of temperature was determined by initially fitting two Voigt profiles to the data with the following free-parameters for each transition: integrated area, collisional width, and line center. The temperature of the gas was then determined using the integrated areas of the transitions. The ratio of the collisional widths and the temperature were averaged over a period where the values were steady for a given test. A linear relationship describing how the ratio of collisional widths varied with temperature was obtained and is given in Eq. 6.

$$\frac{\Delta\nu_c(\text{v"}=1)}{\Delta\nu_c(\text{v"}=0)} = 6.1285\times10^{-5} * T + 0.6950. \tag{6}$$

Constraining the collisional widths to be a temperature-dependent ratio of each other in this manner allowed for more accurate thermometry (see Section VII). This method was necessary because at the high temperatures of interest in this study, much of the O_2 in the air dissociates and reacts to form a gaseous mixture that is no longer air. As a result, the air-broadening parameters provided by HITEMP are not strictly accurate and adjustments to the broadening model were found to be necessary. Thus, a relationship for the ratio of collisional widths, which is independent of pressure, was obtained instead of using individual broadening-coefficients for each transition due to the comparatively large uncertainty in pressure.

VII. Results

Figure 5 shows an example time history of the temperature, pressure, and NO mole fraction measured behind a reflected shock. The colored bands shown for the LAS measurements represent the 95% confidence interval output by the fitting routine. The dashed lines represent the values predicted by NASA CEA. The predictions from NASA CEA were performed using the "shock" mode and based on the initial conditions in the driven section of the shock tube (i.e., T_1 and P_1) and the measured shock speed at the LAS measurement location. It should be noted that this calculation using NASA CEA assumes that for reflected shock cases the gas behind the incident shock reached chemical and thermal equilibrium before the reflected shock passed. Figure 5 (top) shows the pressure measured by the LAS diagnostic and the PCB pressure transducers on the sidewall at the LAS measurement location and the endwall. Not only is the pressure from LAS in reasonable agreement with the pressure transducers, but it also follows a similar trend in time. Figure 5 (bottom) shows the temperature and NO mole fraction measured by the LAS diagnostic in time. The

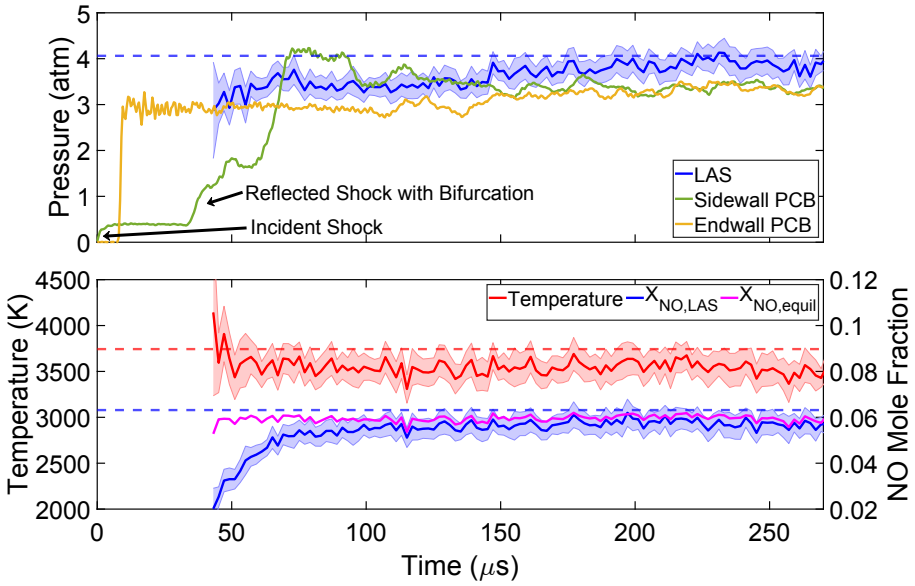

Fig. 5 Time history of pressure (top) and temperature and mole fraction (bottom) measured by the LAS diagnostic as well as predicted values from NASA CEA for equilibrium conditions (red and blue dashed). The magenta line shows the equilibrium NO mole fraction calculated using the temperature and pressure measured by the LAS diagnostic. The pressure traces from the PCB pressure sensors are also included for reference and comparison. The error bands on the LAS measurements indicate the 95% confidence interval output by the fitting routine.

magenta line shows the equilibrium NO mole fraction value calculated at the temperature and pressure measured by the LAS diagnostic at each time. At early times behind the reflected shock, the 500 kHz repetition rate of the LAS diagnostic makes it possible to observe the chemical non-equilibrium in the gas and resolve the temporal evolution of the temperature and NO mole fraction towards their equilibrium values. The temperature immediately behind the shock is largest and the temperature decreases rapidly due to dissociation of the air and endothermic reactions. At these high-pressure and -temperature conditions, vibrational relaxation of NO occurs on a much shorter time scale which could not be resolved by the LAS diagnostic. The decrease in temperature in the first few data points in Figure 5 (bottom) marks the end of the temperature decrease towards equilibrium. Similarly, the formation of NO in time is clearly observable as the mole fraction increases until reaching a steady value at approximately 80 μsec.

For each test, an average value of the measured gas properties was determined after the gas reached a steady-state. Figure 6 shows a summary of the measured gas temperature from the LAS diagnostic compared to the temperature predicted by NASA CEA [40] for each test. The results in Figure 6 show good agreement between the steady-state temperature measured using LAS and the temperature predicted by NASA CEA for both incident and reflected shock cases over temperatures ranging from approximately 2500 to 5500 K. The maximum difference between the measured and predicted equilibrium temperature was 223 K while the mean percent difference was 3.17%. This agreement between the temperature measured by LAS and that predicted by NASA CEA provided confidence in the accuracy of the LAS diagnostic and performance of the HST.

Similar to the temperature measurements, efforts were made to establish confidence in the pressure measured by the LAS diagnostic. This is a challenge as many non-idealities in the flow (e.g., chemical and vibrational non-equilibrium between incident and reflected shock arrival), can result in large differences in pressure compared to those predicted by shock relations. As a result, the pressure predicted by NASA CEA (and shock relations in general) typically was not accurate. As a result, the pressure inferred from LAS was compared to the pressure measured by the PCB pressure transducers in the sidewall and endwall of the HST. For incident shock tests, the sidewall transducers were used for comparison, while for reflected shock tests, a combination of transducers from the sidewall and the endwall were utilized. The measurements from the pressure transducers were used to determine the pressure behind the shock wave and the comparison between the average steady pressure measured by LAS and the pressure transducers is shown in Figure 7 (left). The mean percent difference between the LAS pressure and the pressure measured by the pressure transducers

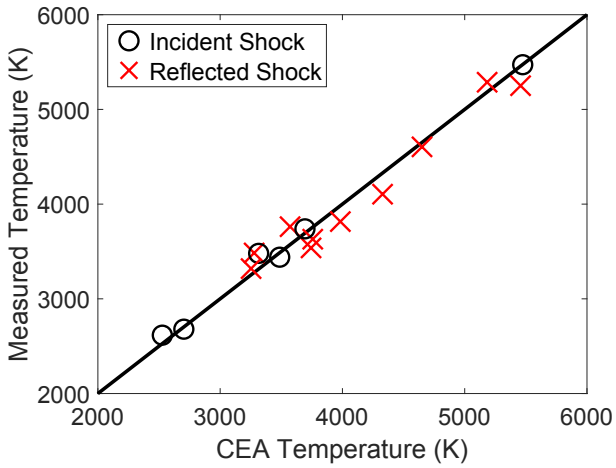

Fig. 6 The average steady-state temperature measured by the LAS diagnostic compared with the temperature predicted by NASA CEA for each test. Measurements were performed behind both incident and reflected shocks.

was 10.8%. While many cases had good agreement between the pressure measured by LAS and the transducers, generally, LAS returned values of pressure that were higher than the transducers. This difference may be due to a number of factors. First, the pressure sensors provided measurements along the shock tube wall, whereas, the LAS measurement is a path integrated measurement along the line of sight. As a result, the pressure sensors could be biased by non-ideal flow effects along the wall, such as shock bifurcation [41]. In addition, the transducers can be biased by many factors including their mounting in the tube and exposure to high temperatures. Second, the LAS diagnostic utilizes the air-broadened collisional broadening parameters for the R(0,36.5) transition given in HITEMP 2019 to infer the pressure. As was discussed in Section V.B., at high temperatures the gas composition changes and is no longer "pure" air. This altered gas composition could alter the collisional width of the NO transitions. Further, at these high temperatures the power-law parameters given in HITEMP may result in significant error. However, despite all these effects, the LAS pressure measurement provides useful data which can be further improved through refinement of the collisional-broadening model.

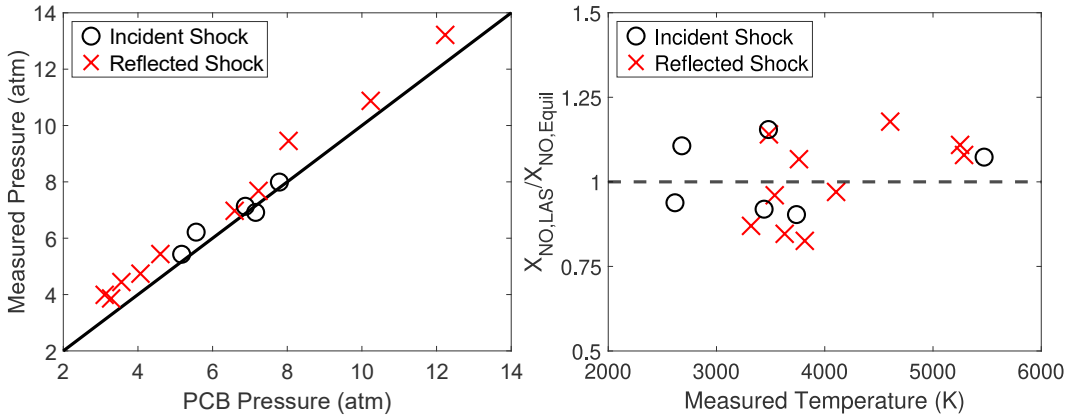

Fig. 7 (Left) The average steady-state pressure measured by the LAS diagnostic compared with the pressure measured by the PCB pressure transducers in the sidewall or endwall of the HST. Measurements were performed behind both incident and reflected shocks. (Right) Ratio of the average steady-state mole fraction of NO measured by the LAS diagnostic to an equilibrium value plotted as a function of the temperature measured by LAS. The equilibrium value of the NO mole fraction was calculated using the average temperature and pressure measured by the LAS diagnostic.

Figure 7 (right) shows the ratio of the average steady-state NO mole fraction measured by the LAS diagnostic to the equilibrium value of NO mole fraction in air calculated at the average steady-state temperature and pressure measured by the LAS diagnostic for each test as a function of the measured temperature. These results show generally good agreement between the LAS measurement and equilibrium values with the ratio for all tests deviating no more than 18%. Disagreement in these results may be due to multiple factors. First, at certain conditions the equilibrium mole fraction of NO in air is very sensitive to the temperature and pressure. Therefore, a small error in either the temperature or pressure could have a significant effect on the calculated equilibrium value of NO mole fraction. In addition, the measured NO mole fraction from LAS is determined from the partial pressure of NO and gas pressure output by the fitting routine discussed in Section V.B. As a result, errors in the pressure measured by LAS will propagate to the mole fraction of NO as well.

VIII. Conclusion

This works presented the development of a high-speed laser-absorption-spectroscopy diagnostic capable of making measurements of temperature, pressure, and NO mole fraction at 500 kHz in high-temperature air. This diagnostic utilized a quantum-cascade laser to measure the absorbance spectra of two fundamental band transitions of NO in the mid-linfrared near 5.06 μm. The 500 kHz measurement rate was achieved through careful selection of the NO transitions utilized, the wavelength tuning characteristics of the laser, and the incorporation of a bias-tee into the circuitry driving the laser current, which circumvented bandwidth limitations of the laser controller. In addition, gas properties were determined using a fitting routine that leveraged a modified form of the time-domain molecular free-induction-decay signal to minimize the impact of measurement errors induced by the assumed incident light intensity.

This diagnostic was successfully applied to make measurements in shock-heated air in the High-Temperature Shock Tube at Sandia National Laboratories at temperatures of 2500 to 5500 K and pressures of 3 to 12 atm. The temperature measured by the LAS diagnostic agreed well with predictions from NASA CEA, while the pressure measurement had generally good agreement with measurements provided by the PCB pressure sensors, thereby giving confidence in the LAS diagnostic. Finally, the rapid measurement rate of the LAS diagnostic was shown to be fast enough to observe chemical non-equilibrium behind the shock wave and well resolve the temporal evolution to equilibrium.

Acknowledgments

This paper describes objective technical results and analysis. Any subjective views or opinions that might be expressed in the paper do not necessarily represent the views of the U.S. Department of Energy or the United States Government. The support of the Laboratory Directed Research and Development program at Sandia National Laboratories is gratefully acknowledged. Sandia National Laboratories is a multimission laboratory managed and operated by National Technology & Engineering Solutions of Sandia, LLC, a wholly owned subsidiary of Honeywell International Inc., for the U.S. Department of Energy's National Nuclear Security Administration under contract DE-NA0003525. Morgan Ruesch was a student at Purdue University while performing this work and was supported by a NASA Space Technology Research Fellowship (Grant 80NSSC18K1174). The authors also thank Anil Nair and Prof. Mitchell Spearrin at UCLA for their guidance in assembling the bias-tee circuitry for the QCL.

References

[1] Anderson Jr, J. D., *Hypersonic and high-temperature gas dynamics*, American Institute of Aeronautics and Astronautics, 2006.

[2] Johnston, C., and Brandis, A., "Modeling of nonequilibrium CO Fourth-Positive and CN Violet emission in CO_2–N_2 gases," *Journal of Quantitative Spectroscopy and Radiative Transfer*, Vol. 149, 2014, pp. 303–317.

[3] Lynch, K. P., and Wagner, J. L., "A free-piston driven shock tube for generating extreme aerodynamic environments," *AIAA SciTech 2019 Forum*, 2019, p. 1942.

[4] Lynch, K. P., Grasser, T., Farias, P., Daniel, K. A., Spillers, R., Downing, C., and Wagner, J. L., "Design and characterization of the Sandia free-piston reflected shock tunnel," *AIAA SciTech 2022 Forum*, 2022.

[5] Nompelis, I., Candler, G. V., and Holden, M. S., "Effect of vibrational nonequilibrium on hypersonic double-cone experiments," *AIAA Journal*, Vol. 41, No. 11, 2003, pp. 2162–2169.

[6] Ruesch, M. D., McDonald, A. J., Mathews, G. C., Son, S. F., and Goldenstein, C. S., "Characterization of the influence of aluminum particle size on the temperature of composite-propellant flames using CO absorption and AlO emission spectroscopy," *Proceedings of the Combustion Institute*, Vol. 38, No. 3, 2021, pp. 4365–4372.

[7] Mathews, G., and Goldenstein, C., "Near-GHz scanned-wavelength-modulation spectroscopy for MHz thermometry and H_2O measurements in aluminized fireballs of energetic materials," *Applied Physics B*, Vol. 126, No. 11, 2020, pp. 1–17.

[8] Goldenstein, C. S., Spearrin, R. M., Jeffries, J. B., and Hanson, R. K., "Infrared laser-absorption sensing for combustion gases," *Progress in Energy and Combustion Science*, Vol. 60, 2017, pp. 132–176.

[9] Miller, J. A., and Bowman, C. T., "Mechanism and modeling of nitrogen chemistry in combustion," *Progress in Energy and Combustion Science*, Vol. 15, No. 4, 1989, pp. 287–338.

[10] Spearrin, R., Schultz, I., Jeffries, J., and Hanson, R., "Laser absorption of nitric oxide for thermometry in high-enthalpy air," *Measurement Science and Technology*, Vol. 25, No. 12, 2014, p. 125103.

[11] Finch, P. M., Girard, J., Strand, C., Yu, W., Austin, J., Hornung, H., and Hanson, R., "Measurements of time-resolved air freestream nitric oxide rotational, vibrational temperature and concentration in the T5 reflected shock tunnel," *AIAA Propulsion and Energy 2020 Forum*, 2020, p. 3714.

[12] Girard, J. J., Finch, P. M., Strand, C. L., Hanson, R. K., Yu, W. M., Austin, J. M., and Hornung, H. G., "Measurements of reflected shock tunnel freestream nitric oxide temperatures and partial pressure," *AIAA Journal*, 2021, pp. 1–10.

[13] Girard, J., Finch, P. M., Schwartz, T., Yu, W., Strand, C. L., Austin, J. M., Hornung, H. G., and Hanson, R. K., "Characterization of the T5 reflected shock tunnel freestream temperature, velocity, and composition using laser absorption spectroscopy," *AIAA Propulsion and Energy 2021 Forum*, 2021, p. 3525.

[14] Lee, M., McMillin, B., Palmer, J., and Hanson, R., "Planar fluorescence imaging of a transverse jet in a supersonic crossflow," *Journal of Propulsion and Power*, Vol. 8, No. 4, 1992, pp. 729–735.

[15] McMillin, B. K., Palmer, J. L., and Hanson, R. K., "Temporally resolved, two-line fluorescence imaging of NO temperature in a transverse jet in a supersonic cross flow," *Applied Optics*, Vol. 32, No. 36, 1993, pp. 7532–7545.

[16] Danehy, P. M., O'Byrne, S., Frank, A., Houwing, P., Fox, J. S., and Smith, D. R., "Flow-tagging velocimetry for hypersonic flows using fluorescence of nitric oxide," *AIAA Journal*, Vol. 41, No. 2, 2003, pp. 263–271.

[17] Jiang, N., Webster, M., Lempert, W. R., Miller, J. D., Meyer, T. R., Ivey, C. B., and Danehy, P. M., "MHz-rate nitric oxide planar laser-induced fluorescence imaging in a Mach 10 hypersonic wind tunnel," *Applied Optics*, Vol. 50, No. 4, 2011, pp. A20–A28.

[18] Hanson, R., Monat, J., and Kruger, C., "Absorption of CO laser radiation by NO," *Journal of Quantitative Spectroscopy and Radiative Transfer*, Vol. 16, No. 8, 1976, pp. 705–713.

[19] Monat, J., Hanson, R., and Kruger, C., "Shock tube determination of the rate coefficient for the reaction N_2+ O $\rightarrow$ NO+ N," *Symposium (International) on Combustion*, Vol. 17, No. 1, 1979, pp. 543–552.

[20] Falcone, P., Hanson, R., and Kruger, C., "Tunable diode laser absorption measurements of nitric oxide in combustion gases," *Combustion Science and Technology*, Vol. 35, No. 1-4, 1983, pp. 81–99.

[21] Falcone, P., Hanson, R., and Kruger, C., "Tunable diode laser measurements of the band strength and collision halfwidths of nitric oxide," *Journal of Quantitative Spectroscopy and Radiative Transfer*, Vol. 29, No. 3, 1983, pp. 205–221.

[22] von Gersum, S., and Roth, P., "IR-diode laser measurements on the decomposition of NO behind shock waves," *Experiments in Fluids*, Vol. 13, No. 5, 1992, pp. 299–304.

[23] Mohamed, A., Rosier, B., Henry, D., Louvet, Y., and Varghese, P., "Tunable diode laser measurements on nitric oxide in a hypersonic wind tunnel," *AIAA Journal*, Vol. 34, No. 3, 1996, pp. 494–499.

[24] Oh, D. B., and Stanton, A. C., "Measurement of nitric oxide with an antimonide diode laser," *Applied Optics*, Vol. 36, No. 15, 1997, pp. 3294–3297.

[25] Mihalcea, R. M., Baer, D. S., and Hanson, R. K., "A diode-laser absorption sensor system for combustion emission measurements," *Measurement Science and Technology*, Vol. 9, No. 3, 1998, p. 327.

[26] McCurdy, M., Bakhirkin, Y., and Tittel, F., "Quantum cascade laser-based integrated cavity output spectroscopy of exhaled nitric oxide," *Applied Physics B*, Vol. 85, No. 2, 2006, pp. 445–452.

[27] Parker, R., Wakeman, T., Holden, M., and MacLean, M., "Measuring nitric oxide freestream concentration using quantum cascade lasers at CUBRC," *44th AIAA Aerospace Sciences Meeting and Exhibit*, 2006, p. 926.

[28] Parker, R., Wakeman, T., MacLean, M., and Holden, M., "Measuring nitric oxide freestream velocity using quantum cascade lasers at CUBRC," *45th AIAA Aerospace Sciences Meeting and Exhibit*, 2007, p. 1329.

[29] Chao, X., Jeffries, J. B., and Hanson, R. K., "In situ absorption sensor for NO in combustion gases with a 5.2 μm quantum-cascade laser," *Proceedings of the Combustion Institute*, Vol. 33, No. 1, 2011, pp. 725–733.

[30] Almodovar, C. A., Spearrin, R. M., and Hanson, R. K., "Two-color laser absorption near 5 μm for temperature and nitric oxide sensing in high-temperature gases," *Journal of Quantitative Spectroscopy and Radiative Transfer*, Vol. 203, 2017, pp. 572–581.

[31] Almodovar, C. A., Su, W.-W., Strand, C. L., and Hanson, R. K., "R-branch line intensities and temperature-dependent line broadening and shift coefficients of the nitric oxide fundamental rovibrational band," *Journal of Quantitative Spectroscopy and Radiative Transfer*, Vol. 239, 2019, p. 106612.

[32] Hanson, R. K., Spearrin, R. M., and Goldenstein, C. S., *Spectroscopy and optical diagnostics for gases*, Springer, 2016.

[33] Cole, R. K., Makowiecki, A. S., Hoghooghi, N., and Rieker, G. B., "Baseline-free quantitative absorption spectroscopy based on cepstral analysis," *Optics Express*, Vol. 27, No. 26, 2019, pp. 37920–37939.

[34] Goldenstein, C. S., Mathews, G. C., Cole, R. K., Makowiecki, A. S., and Rieker, G. B., "Cepstral analysis for baseline-insensitive absorption spectroscopy using light sources with pronounced intensity variations," *Applied Optics*, Vol. 59, No. 26, 2020, pp. 7865–7875.

[35] Li, J., Schwarm, K. K., Wei, C., and Spearrin, R. M., "Robust cepstral analysis at variable wavelength scan depth for narrowband tunable laser absorption spectroscopy," *Measurement Science and Technology*, Vol. 32, No. 4, 2021, p. 045502.

[36] Rothman, L. S., Gordon, I., Barber, R., Dothe, H., Gamache, R. R., Goldman, A., Perevalov, V., Tashkun, S., and Tennyson, J., "HITEMP, the high-temperature molecular spectroscopic database," *Journal of Quantitative Spectroscopy and Radiative Transfer*, Vol. 111, No. 15, 2010, pp. 2139–2150.

[37] Hargreaves, R. J., Gordon, I. E., Rothman, L. S., Tashkun, S. A., Perevalov, V. I., Lukashevskaya, A. A., Yurchenko, S. N., Tennyson, J., and Müller, H. S., "Spectroscopic line parameters of NO, NO_2, and N_2O for the HITEMP database," *Journal of Quantitative Spectroscopy and Radiative Transfer*, Vol. 232, 2019, pp. 35–53.

[38] Tennyson, J., Yurchenko, S. N., Al-Refaie, A. F., Barton, E. J., Chubb, K. L., Coles, P. A., Diamantopoulou, S., Gorman, M. N., Hill, C., Lam, A. Z., et al., "The ExoMol database: molecular line lists for exoplanet and other hot atmospheres," *Journal of Molecular Spectroscopy*, Vol. 327, 2016, pp. 73–94.

[39] Nair, A. P., Lee, D. D., Pineda, D. I., Kriesel, J., Hargus, W. A., Bennewitz, J. W., Danczyk, S. A., and Spearrin, R. M., "MHz laser absorption spectroscopy via diplexed RF modulation for pressure, temperature, and species in rotating detonation rocket flows," *Applied Physics B*, Vol. 126, No. 8, 2020, pp. 1–20.

[40] Gordon, S., and McBride, B. J., "Computer program for calculation of complex chemical equilibrium," *NASA reference publication*, Vol. 1311, 1994.

[41] Petersen, E., and Hanson, R., "Measurement of reflected-shock bifurcation over a wide range of gas composition and pressure," *Shock Waves*, Vol. 15, No. 5, 2006, pp. 333–340.